Theoretical studies of molecular scale near-field electron dynamics

Roi Baer[a)]
Department of Physical Chemistry and the Lise Meitner Center for Quantum Chemistry,
The Hebrew University of Jerusalem, Jerusalem 91904, Israel

Daniel Neuhauser[b)]
Department of Chemistry and Biochemistry, University of California at Los Angeles, California 90025-1569

Near-field scanning microscopy and nonlinear spectroscopy on a molecular scale involve weakly interacting subsystems that dynamically exchange electrons and electromagnetic energy. The theoretical description of such processes requires unified approach to the electron-near-field dynamics. By considering electronic structure and dynamics of two distant clusters or atoms we show that adiabatic local spin-density approximation (ALSDA) fails to describe (even qualitatively) essential details of electron dynamics in weakly interacting systems. A recently developed functional addresses these ailments within a time-dependent setting. With this method we study the spectroscopy of a composite system, namely, two weakly coupled metallic clusters. The near-field (dipole-dipole) coupling and electron transfer display an interesting interplay, producing exponential sensitivity of emission yield to the intercomponent distance. © *2006 American Institute of Physics.*
[DOI: 10.1063/1.2335841]

I. INTRODUCTION

Nanometer-scale characterization and control of materials, catalytic processes, interfaces, and nanostructures are of prime importance in materials science and related technology. A suite of techniques that enable such feats is obtained by combining near-field methods[1,2] with molecular spectroscopy.[3–5] Near-field scanning optical microscopy (NSOM) makes use of subwavelength light sources and scanning probes, producing images with resolution well beyond the diffraction limit.[5,6] Such techniques are routine in various fields in chemistry, biology, and materials science.[7–11] An impressively large body of theoretical work forms the basis for interpreting and understanding NSOM measurements. Aiming at image prediction and interpretation,[4,6,12–20] the focus is on the electromagnetic field. Matter is less important at length scales much beyond 10 nm and can thus be described using a Drude model.[21] This is appropriate when the external fields are sufficiently weak to suppress nonlinear responses. Such NSOM theories therefore apply for systems with length scale $\geqslant 10$ nm. Yet smaller length scales are vigorously pursued as molecular resolution is becoming available using smaller tips and probes.[22–26] Here, new challenges emerge. Interpretation of near-field measurements is complex due to the proximity of the subsystems, which enables electron transfer reactions to take place. Furthermore, manipulating and controlling near fields on the molecular scale are challenging. One example is the need for accurate delivery of electromagnetic energy to specific locations in a nanometric system. Experimental progress in this direction was made recently by coupling optical light to the collective electronic charge oscillations (localized surface plasmons) near metallic surfaces[10,27] or by propagating light through crystalline nanowires.[28,29]

It is possible to go beyond the Drude model and treat the near field and the electron dynamics in a more balanced way using the time-dependent density functional theory (TDDFT). A similar idea was suggested long ago, where a predecessor of TDDFT, the electron gas random phase approximation (RPA), was used to study the dynamics of electromagnetic near fields at surfaces and inside metals.[30] In applications such as excited states in molecules and metallic clusters TDDFT delivers a good combination of accuracy and efficiency.[31] However, as we show below, typical local functionals (including RPA) are unsuitable for treating weakly coupled systems which is our focus here. Instead, most applications use TDDFT within linear-response theory in the frequency domain. [32–35] TDDFT in *real time*[36–43] is a less common approach, although it has a wider scope of applicability and it can go beyond linear response. We will use time-dependent methods in this paper. A growing number of applications of TDDFT are in the domain of strong laser fields.[44–48] TDDFT is also useful for studying the dynamics of electrons in small metal clusters and nanodots.[35,41,49–52]

In this article, we develop a theory for molecular scale near fields based on TDDFT. Applying TDDFT to this problem is not trivial. Functionals such as the adiabatic local spin-density approximation (ALSDA) are often successful for excited electronic states of molecules and clusters but are inappropriate for weakly coupled systems. We developed a functional for overcoming the long-range self-interaction problem plaguing local functionals in DFT and TDDFT.[53] An important paper developed a similar approach to long-range correction functionals[54] leading to more consistent dipole moments, polarizabilities, and hyperpolarizabilities of push-

---

[a)]Electronic mail: roi.baer@huji.ac.il
[b)]Electronic mail: dxn@chem.ucla.edu

© 2006 American Institute of Physics

pull π-conjugated systems.[55] We explain here why these approaches are necessary for a correct qualitative behavior of weakly coupled systems.

Using the new theory, we study in detail a simple model for a near-field microscope: a system consisting of two weakly coupled metallic entities having variable distance. We subject this composite system to a short ultraviolet laser pulse, showing that the induced emission is sensitive to the tip-substrate distance. There is growing experimental interest in "nanometric rulers" of this type.[56–60] Even though our original driving field is not a "near field," the induced charge oscillations and currents in each part generate electrical fields that affect all other parts. At long distances, such an interaction is predominantly dipole-dipole. However, at small distances, and in the presence of bias potentials, other effects may be important. These include overlap or charge transfer effects as well as screening in metallic systems. The various parts of the system create and react to local near fields. As the two subsystems approach, electron currents can form between them and new effects kick in; these merging subsystems rapidly change their spectroscopic behavior. It is possible to find transitions that display dramatic changes in the absorption and emission properties in response to small variations of the distances.

We present the theory for computing near field on the molecular scale in Sec. II, followed by the application in Sec. III. A summary and discussion then follows in Sec. IV. We add an appendix with the details of the new functional.

II. THEORY

We consider here the response properties of a composite system consisting of two well-separated, weakly interacting subsystems. We wish to determine the emission response of the system on exposure to electromagnetic far-field radiation. This response is dependent on a complex series of physical processes. Not only do we have to compute the quantum dynamics of the electrons localized in each subsystem, based on the external electromagnetic fields, but we need also to take account of the near-field interaction between the subsystems. In weakly coupled subsystems, the new complication is the tendency of electrons to localize in subsystems. Therefore, *long-range interactions* play an important role. This is a weakness of the local functionals often used in TDDFT [such as ALSDA, generalized gradient approximation (GGA), and even the simpler RPA]. For single entity systems, ALSDA is often a good theory. However, as we show in Secs. II A and II B, for composite systems it may not even be *qualitatively* correct. In Sec. II C, we discuss a long-range self-interaction correction, allowing for a qualitatively correct long-range interaction.

Let us briefly cover a few methodological and numerical details on the calculations reported in this paper. The electronic structure and dynamical calculations employ a plane-wave basis-set method and the jellium calculations use a simulation cell size of $20 \times 20 \times 72 a_0^3$ and cutoff kinetic energy of $1.2 E_h$. We used an image screening technique to isolate the cell.[61] For the time-dependent calculations, a fifth order adaptive Runge-Kutta method[62] solves the time-dependent Kohn-Sham (KS) equations.

A. Charge quantization and derivative discontinuities

The local spin-density approximation (LSDA) involves the use of the polarized homogeneous gas exchange- correlation (XC) energy as a local functional of the density $E_{XC}^{hom}[n_\uparrow, n_\downarrow]$. This functional replaces the exact XC functional of DFT in the Kohn-Sham equations.[63] This approximation often leads to accurate estimates of the electron spin densities $n_\uparrow(\mathbf{r})$ and $n_\downarrow(\mathbf{r})$ [where $\mathbf{r}$ denotes a point in three-dimensional (3D) space] in strongly interacting, chemically bound systems. However, in composite systems this is not usually the case. Suppose a LSDA calculation yields a good approximation to the ground-state densities $n_A(\mathbf{r})$ and $n_B(\mathbf{r})$ of systems A and B separately (for clarity, we suppress the spin indices in this discussion). Furthermore, suppose the two densities are localized in two well-separated regions, so they are nonoverlapping. Then, the extensive nature of the energy demands that $E_{gs}[AB] = E_{gs}[A] + E_{gs}[B]$. However, the KS energy within the LSDA does not obey this constraint.[53] This is surprising, since the LSDA XC energy functional is strictly additive: $E_{XC}^{hom}[n_A + n_B] = E_{XC}^{hom}[n_A] + E_{XC}^{hom}[n_B]$.

This problem is a result of the combination of the variational KS approach and the LSDA XC functional. This blend tends to produce electron densities that violate the principle of charge quantization, namely, that each subsystem has an integer number of electrons. Thus, the electron density n_A changes when system B is introduced no matter how far it is and even though they should be physically noninteracting. For example, consider the simplest one-electron system, H_2^+. One nucleus, we label A is at a point $\tilde{\mathbf{R}}/2$ and the other, B at $-\tilde{\mathbf{R}}/2$, so the distance between the two nuclei is $\tilde{R}$. We assume $\tilde{R}$ is large. For the electron, a symmetric double well forms. The two $1s$ states in each well combine to form two molecular orbitals with minute tunneling splitting $\Delta \propto \exp[-\tilde{R}/a_0] \rightarrow 0$. The ground-state density of the electron in this double well delocalizes over the two wells, and at very large $\tilde{R}$:

$$n(\mathbf{r}) = [n_{1s}(\mathbf{r} + \tilde{\mathbf{R}}/2) + n_{1s}(\mathbf{r} - \tilde{\mathbf{R}}/2)]/2. \tag{2.1}$$

This delocalization exists only when exceptional symmetric conditions prevail. Large values of $\tilde{R}$ destroy the localization because of the high sensitivity to fluctuations. Indeed, consider a small change in the surrounding, which biases one of the nuclei (say A), changing its energy by a small amount ε with $|\varepsilon| > \Delta$. It is obvious that the density response of the system will be dramatic since the electron will localize in the lower energy well:

$$n_\varepsilon(\mathbf{r}) = n(\mathbf{r} - \tilde{\mathbf{R}}/2) + O(\Delta),$$

$$\tag{2.2}$$

$$n_{-\varepsilon}(\mathbf{r}) = n(\mathbf{r} + \tilde{\mathbf{R}}/2) + O(\Delta).$$

As $\tilde{R}$ grows, this relation exponentially becomes a "density discontinuity," where a minute change in the bias causes a

huge large change in the ground-state density. This is the source of "derivative discontinuities"[64] in the XC functionals of many-electron systems.

In many chemical systems, even the simplest ones, local density functionals violate harshly the charge quantization rule and fail to display or approximate the required derivative discontinuity.[53] As an example, consider a widely spaced hydrogen-nitrogen cationic system, denoted $[H\ldots N]^+$, and suppose that for definiteness the interatomic distance is 10 Å. The ionization potential of the nitrogen atom is higher than that of hydrogen by 1 eV. Thus, in the ground state this system consists of a neutral nitrogen atom and a bare proton 10 Å away. Yet the LSDA calculation (with spin z component$=3/2$) finds the two species share electrons. The average electronic charge near the nitrogen atom in LSDA is $6.6e$ and near the proton is $0.4e$. Furthermore, the energy is asymptotically Coulombic proportional to $\widetilde{\mathbf{R}}^{-1}$. This "bond energy" is the same no matter how far the systems are.

This false behavior of LSDA exists in many weakly coupled systems. Sometimes the problem is not dramatic. For example, in $[H\ldots F]^+$ with a HF distance of 10 Å the charge on the more electronegative fluorine atom is $8.97e$, that is close to $9e$ and on the proton $0.03e$–close to 0.

We note that this malady of LSDA is an expression of spurious long-range self-interaction and therefore plagues all local functionals, such as GGA.

B. Problem of ALSDA for weakly coupled systems

The approximation where LSDA is used as an instantaneous XC functional in TDDFT is called the *adiabatic* LSDA.[32] We now wish to study ALSDA for weakly interacting systems. We consider a system of metallic character, namely, two separated metallic jellium spheres. A jellium sphere is simply a static smeared positive charge in the form of a sphere with electrons added to it. For example, a sphere centered at the origin of radius a and density n_0 is described by the following positive charge distribution:

$$n_+(\mathbf{r}) = \frac{n_0}{1 + e^{(r-a)/w}}. \tag{2.3}$$

The sphere radius a is chosen such that the total charge, $\int n_+(\mathbf{r})d^3r=N_+$, is an integer. The parameter w is a smoothing parameter that prevents abrupt discontinuity of the density at the jellium surface; its value in all calculations we present below is $w=0.4a_0$. Such spheres are good approximations for clusters of alkali metals.[65,66] The density n_0 determines the "material" the sphere is made of. We consider two such spheres, each containing eight nuclei (i.e., having $N_+=8$ charges). One sphere is made of a high density material, such as aluminum, with a density of $0.03a_0^{-3}$. The other sphere can be thought of as made of silver (although silver is not an alkali metal) with a density of $0.0088a_0^{-3}$. Below we refer to the high density sphere as H (hard) and the low density sphere as S (soft). The relevant characteristics of the spheres are given in Table I.

We performed separate LSDA calculations on each sphere and determined its ionization potentials (IPs). Note that in DFT one can determine the ionization potential in (at

TABLE I. The parameters and calculated properties of the H and S jellium spheres.

Property/Parameter			H sphere	S sphere
Basic density n_0/a_0^{-3}			0.03	0.0088
Radius a/a_0			4	6
Total positive charge N_+			8	8
Ionization potential (IP) (eV)	LSDA	ΔSCF	7.1	5.5
		HOMO	4.7	3.6
	$\gamma=1$	ΔSCF	6.5	4.9
		HOMO	7.1	5.4

least) two ways: either as the difference between the ground-state energies of the neutral and the ion (ΔSCF) or as the energy of the highest occupied molecular orbital (HOMO).[67] The ionization results for the LSDA are both shown in Table I. Note that the two types of IP estimates come out in LSDA very different. This is a known defect of LSDA. One sees that the IP of the H sphere is higher by 1.6 eV than that of the S sphere. This means that the ground state of the weakly coupled cation $[H\ldots S]^+$ is $H\ldots S^+$. However, a LSDA calculation of a combined system, where both spheres are present but far from each other, does not bear this out. It turns out that the charge on the H sphere is $7.8e$ while on the S sphere is $0.2e$. This means that LSDA does not predict the correct charge distribution for this system to start with. This is similar to the nitrogen-hydrogen cation we considered in Sec. II A.

The conclusion is that the initial charge distribution and the Kohn-Sham orbitals of LSDA are not a proper starting point for TDDFT. To see the consequence of starting with a wrong initial distribution, let us consider the absorption spectrum of the $[H\ldots S]^+$ system. First, take each subsystem separately. There are four components: H, H^+, S, and S^+. We compute their photoabsorption spectra within ALSDA in the following way. We expose the system to a short Gaussian electric field pulse:

$$E(t) = E_0 e^{-(t-T)^2/2\sigma^2} \cos \omega t, \tag{2.4}$$

with $E_0=10^{-4} E_h(ea_0)^{-1}$, $T=8\hbar E_h^{-1}$, $\sigma=2\hbar E_h^{-1}$, and $\omega=0 E_h\hbar^{-1}$. The field couples to the system via the electronic dipole operator. Because of this time-dependent perturbation, the system is set into motion and we record the electronic dipole moment $\mathbf{d}(t)=\int n(\mathbf{r},t)\mathbf{r}d^3r$ at constant intervals of time. Fourier analysis of this transient gives the absorption cross section or the emission yields as a function of frequency.[39,43] The results for the four types of spheres are shown in Fig. 1. It is interesting to note that the absorption spectrum of the cationic system is dominated by a single absorption line while the neutral system has several lines of comparable strengths.

Physical intuition has it that the photoabsorption cross section of the $[H\ldots S]^+$ system, given in Fig. 2, should resemble the combination of the H and S^+ spectrum although lines may shift a little due to weak interactions between the spheres (the sphere centers are $24a_0$ apart). An inspection of Fig. 2 reveals that indeed the strongest lines are due to H and S^+ spheres but these are shifted quite a bit. For example, the
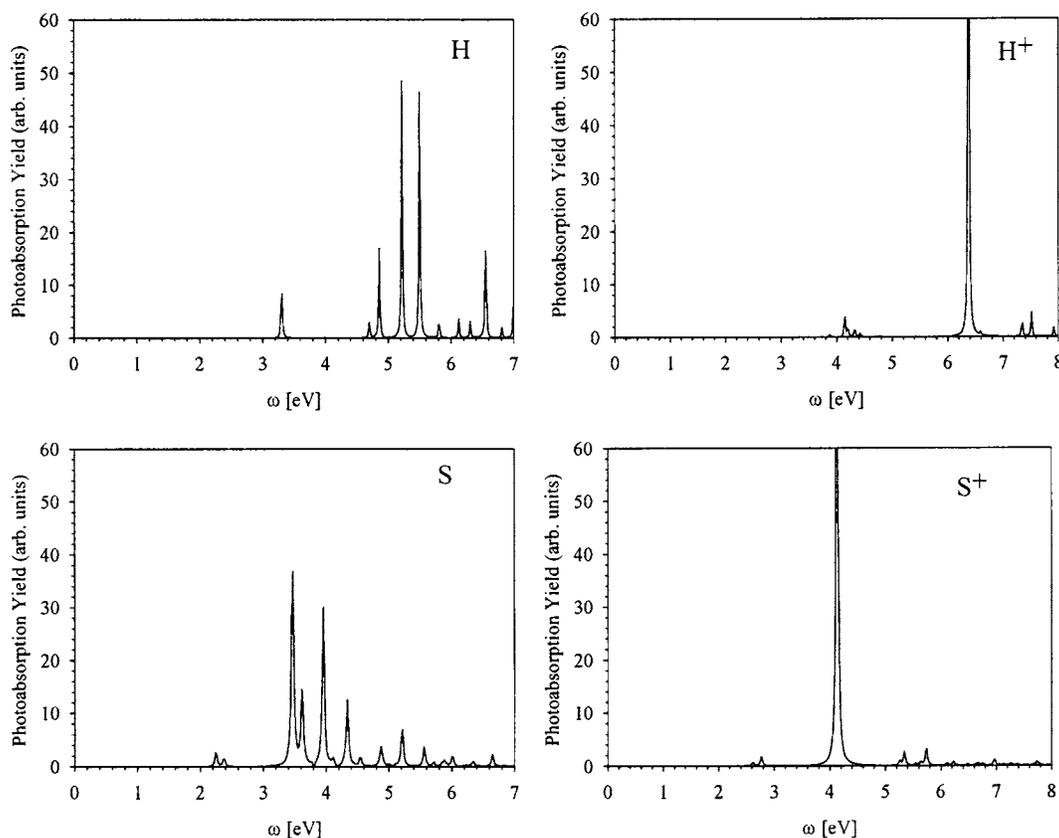
FIG. 1. The LSDA photoabsorption spectrum for the H, H$^+$, S, and S$^+$ systems.

line of the isolated S$^+$ sphere at 4.13 eV is redshifted in the presence of the H sphere to 3.99 eV, as shown in Fig. 2. The 3.31 eV line of the isolated H sphere is blueshifted to 3.55 eV in the presence of S$^+$. We have built a table of the transition lines of the isolated H and S$^+$ spheres and the combined [H...S]$^+$ system for a large separation (of $24a_0$). The assignment of a spectral line in the composite system considers the location with respect to the separate sub-systems and their response to a localized bias potential as described below. The lines in the 5–6 eV range are difficult to assign because both spheres have spectral lines in this range so there is strong dipole coupling (see below).
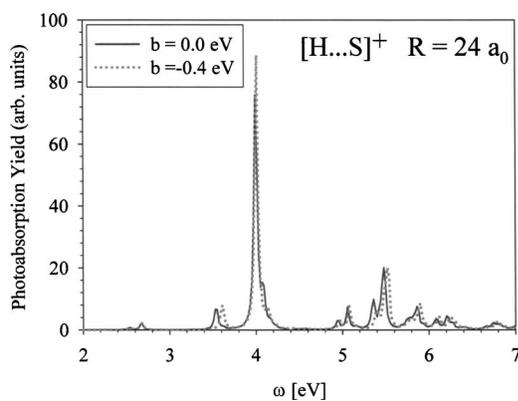

FIG. 2. The LSDA absorption spectrum of the [H...S]$^+$ system at $R=24a_0$.

Let us now also study the effect of a local perturbation on one of the spheres on the combined spectrum. We apply a small bias potential on the H sphere. The functional form of this bias potential is

$$u_{\text{bias}}(\mathbf{r}) = \frac{b}{1 + e^{(|\mathbf{r}-\mathbf{R}_H|-a)/w}}, \quad b = -0.4 \text{ eV}, \tag{2.5}$$

where $\mathbf{R}_H$ is the radius vector to the center of the H sphere. This potential affects only electrons in the H sphere, and not in the S$^+$ sphere. It deepens the external electrostatic potential in the H sphere making the potential gradient steeper. An electron in the H sphere thus feels a stronger localizing force at the sphere surface. Upon application of the bias, the transitions associated with the H sphere will therefore slightly shift to the blue while those associated with the S sphere should be unaffected. In Fig. 2, we observe that this behavior is approximately obeyed. Lines associated with internal transitions in the H sphere are blueshifted by 0.07 eV, while those corresponding to internal transitions in the S$^+$ sphere are blueshifted by 0.02 eV.

Summarizing, we find two problems with the ALSDA functional when treating weakly coupled systems:

(1) The spectral lines are shifted considerably. In our case the lines of the H sphere are shifted to the blue by more than 0.2 eV and those originating in the S$^+$ sphere are shifted to the red by more than 0.1 eV. This is a direct result of the partial, noninteger charge transfer.

(2) The lines of the S$^+$ sphere are too sensitive to the local bias exerted on the H sphere. This sensitivity is not
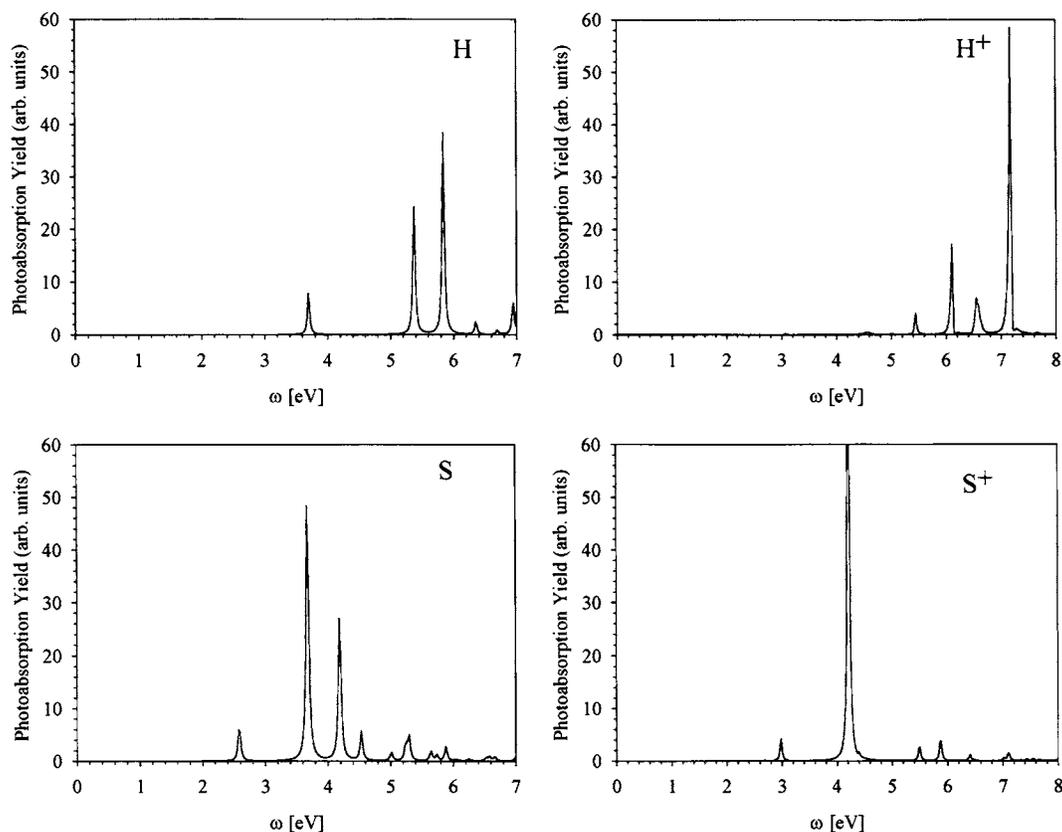
FIG. 3. The $\gamma=1$ photoabsorption spectrum for the H, H$^+$, S, and S$^+$ systems.

physical and is again a result of the partial charge transfer, which makes the system too "ultranonlocal."

We now show how to eliminate these problems by using a long-range self-repulsion corrected functional.

C. Long-range self-repulsion correction

The ailments of ALSDA discussed above are all associated with the self-repulsion problem: each electron repels itself, so it is energetically advantageous for the Kohn-Sham orbitals to delocalize between the two atoms or metal clusters, causing false charge sharing. Furthermore, the same problem has the result that in ALSDA the energy required for charge transfer excitations is much too small.[68]

Recently we described[53] a functional with the correct long-range behavior which introduces in a rigorous manner a long-range correction through a new density functional $\gamma[n]$. Details of the functional are given in the Appendix. Using this functional we obtain the ionization energies shown in Table I. These are similar to the LSDA values, but notice that the HOMO energies are much closer to the ionization energies. Furthermore, when the ground state of the [H...S]$^+$ system is computed the resulting charge distribution yields integer values for the charge on each subsystem: eight electrons on the H sphere and seven electrons on the S sphere.

In order to study the performance of the new functional for the response properties of the weakly coupled systems, consider the photoabsorption spectrum, as computed for each

sphere in Fig. 3, and for the combined [H...S]$^+$ system at $R=24a_0$ in Fig. 4. When comparing to the results of the ALSDA functional, one should note two striking differences.

(1) The absorption lines of the combined system in Fig. 4 are almost exactly the same as those of the separate systems in Fig. 3, except for lines which interact electromagnetically in the range of 5–6 eV, discussed below.

(2) There is a complete indifference of the levels on the S$^+$ sphere to the localized bias potential exerted on the H sphere. This is physical and unlike in the ALSDA case, where the S$^+$ sphere is affected (although less than the H sphere itself).
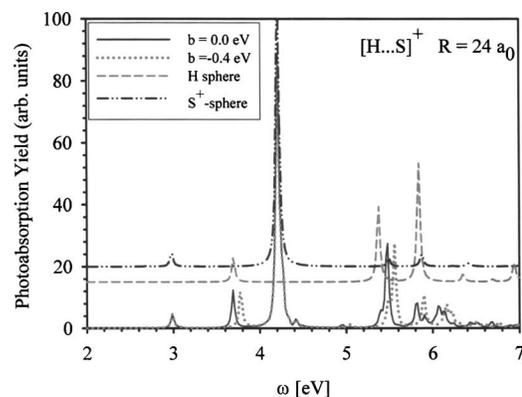

FIG. 4. The $\gamma=1$ absorption spectrum of the [H...S]$^+$ system at $R=24a_0$.

Thus we find that the new functional is better suited to study the spectrum of weakly coupled systems, as it gives correct qualitative behavior.

D. Dipole-dipole coupling

Lastly, we discuss the phenomenon of dipole coupling which is seen in the 5–6 eV range where the two spheres have similar absorption lines. The TDDFT calculations we present already take account of this phenomenon (except for retardation effects, which are negligible on this scale). In order to understand why the line positions and intensities are sensitive to the distance R we invoke the well known theory of dipole-dipole coupling due to Eisenschitz and London.[69]

Consider two coupled spectroscopic lines, one on each subsystem, with similar frequencies ω_i, where $i=$H, S$^+$. The dipole coupling is $C \approx d_H d_{S^+}/R^3$, where d_i is the relevant transition dipole moment on each sphere. The resulting spectral lines can be determined by diagonalizing a 2×2 matrix, giving frequencies

$$\Omega_\pm = \bar{\omega} \pm \sqrt{\Delta^2 + C^2}, \qquad (2.6)$$

where $\Delta=(\omega_H - \omega_{S^+})/2$ and $\bar{\omega}=(\omega_H + \omega_{S^+})/2$ and an overall transition dipole for each line:

$$\begin{pmatrix} D_+ \\ D_- \end{pmatrix} = \begin{pmatrix} \cos\theta/2 & \sin\theta/2 \\ -\sin\theta/2 & \cos\theta/2 \end{pmatrix} \begin{pmatrix} d_H \\ d_{S^+} \end{pmatrix}, \qquad (2.7)$$

where $\tan\theta=C/\Delta$. When $|\Delta|$ is much larger than $|C|$ the energy level splitting $\Omega_+ - \Omega_-$ is sensitive to C^2/Δ proportional to R^{-6}. But when $|\Delta|$ is much smaller, the splitting is proportional to $|C|$, i.e., R^{-3}. In this latter case θ is close to $\pi/2$ (assuming $C>0$) and we find large attenuation of the total transition dipole: D_+ is the sum of the dipoles (super-radiance) and D_- is their difference (subradiance).

In our case, C is of the order of 0.05 eV and in the 5–6 eV range there are two pairs of transitions (at least) that can interact quite strongly via the dipole coupling. Thus, the combined spectrum is sensitive to the distance between the spheres. As discussed below, when this distance is further reduced by 1.5 Å an additional phenomenon comes in—charge transfer and direct (overlap) interaction. To account for this in the above two-level theory, we can change C.

III. DISTANCE SENSITIVE EMISSION YIELD

In the previous section, we studied a TDDFT functional which is appropriate for describing a composite system consisting of weakly coupled components. In the [H…S]$^+$ system we considered, we found strong dipole-dipole coupling between the two spheres for transitions in the 5–6 eV range. Here, we investigate the consequences of this in more detail. We first discuss the absorption spectrum and then show an application where the dipole coupling affects the emission.

The absorption spectrum of the two-sphere system in the 5–6 eV range as a function of the distance between the spheres is shown in Fig. 5. One sees that the position and strength of the absorption lines are very sensitive to the distance R. This can be explained in terms of the dipole-dipole interaction discussed in Sec. II D, where we found that an absorption line ω_1 on the H sphere can combine with a line
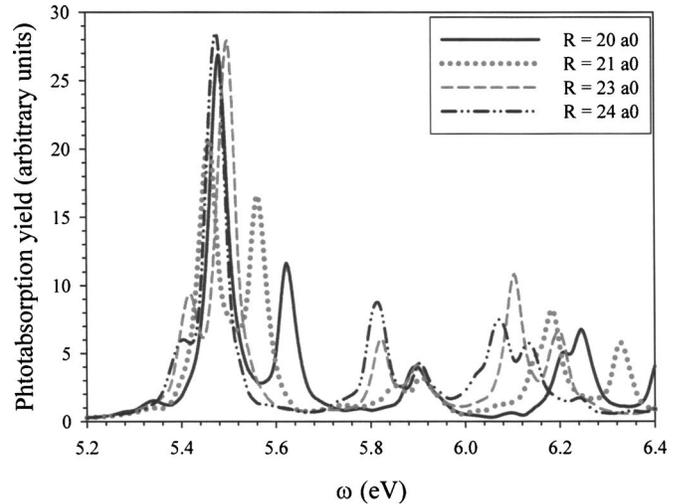

FIG. 5. The absorption spectrum of the [H…S]$^+$ system for several distances.

ω_2 of the S$^+$ sphere to give a pair of "dressed" lines given by (2.6). When the frequency difference Δ is comparable to the dipole-dipole coupling C the position and yield of the new lines will be sensitive to C, or since $C \propto R^{-3}$ to the distance R.

As a result, one can easily find, for small enough R, an absorption line of [H…S]$^+$, such as 5.6 eV, which is *not* an absorption line of the H sphere or the S$^+$ sphere separately. Illuminating the system in this frequency will result in a sensitive probe: the emission yield will be sensitive to the distance R. In Fig. 6 we plot the emission yield following exposure to a 5 fs Gaussian pulse of frequency 5.6 eV. We used the electric field given in Eq. (2.4), with $E_0=10^{-4} E_h(ea_0)^{-1}$, $T=600\hbar E_h^{-1}$, $\sigma=200\hbar E_h^{-1}$, and $\omega=0.206 E_h\hbar^{-1}$. During and after the application of the pulse we computed the time-dependent dipole moment from which the emission yield is deferred. The total emission in the 5–6 eV interval is shown in Fig. 7 as a function of R. The emission yield increases by an order of magnitude as the distance changes from $26a_0$ to $21a_0$. We find emission extremely sensitive to R and angstrom resolution is possible.

Since the spheres approach each other quite significantly, a question may be raised as to the role of charge transfer and "overlap" of the electronic clouds in shifting the lines. The sharp response to the distance is indicative of an exponential
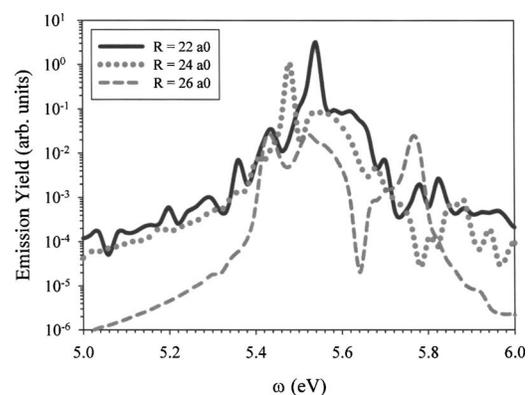

FIG. 6. The 5.6 eV stimulated emission as a function of the distance between the spheres.
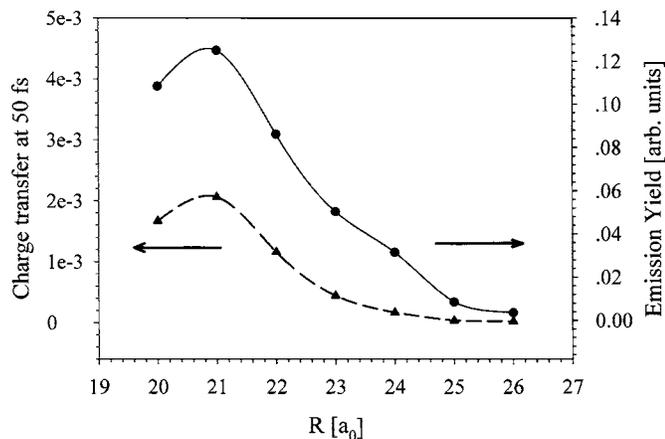
FIG. 7. The stimulated emission yield (at 5.6 eV) and the charge transferred as a function of distance R (lines are shown as a guide to the eye).

dependence of the coupling on the distance. In Fig. 7 we observe charge being transferred from the H to the S^+ sphere. This sets in concurrently with the steep rise in emission yield. This indicates that significant overlap or direct interactions are becoming important. However, it is difficult to assess the rate of charge transfer because of the weak pulses being used (the amount of excitation is very small to begin with).

The temporal dynamics of the charge transfer is studied in Fig. 8 for several intersphere distances R (these are filtered transients, where high-frequency oscillations were eliminated). Notice that charge transfer appears tens of femtoseconds after the pulse is over. Concluding this section, we have shown that it is possible to achieve a fine (angstrom) distance sensitivity by monitoring the emission yield following excitation by a short Gaussian pulse.

IV. SUMMARY AND DISCUSSION

We studied here some aspects of the electronic spectroscopy of a system composed of two weakly coupled entities. ALSDA, which is useful in other contexts, was shown here to be unsuitable because it harnesses self-interaction, causing unphysical ultra-non-local coupling between the two entities. We then considered a new functional for TDDFT and we demonstrated that it overcomes these difficulties. Using the
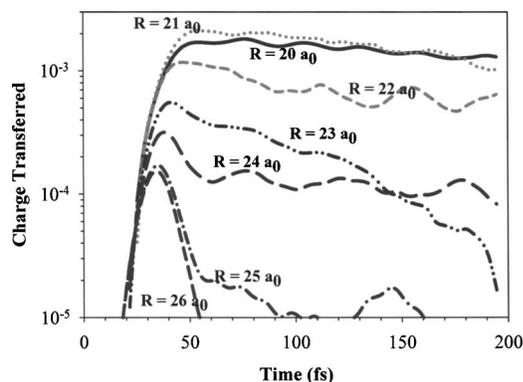

FIG. 8. The smoothed transient of charge transfer following exposure to a weak 5 fs pulse at a frequency of 5.6 eV as a function of time for several distances R.

new theory, we studied the spectroscopy of a composite system of two weakly coupled spherical metal clusters as a function of their distance.

The new functional will be useful to describe many processes in near-field molecular and molecular electronics applications. Specifically, conductivity of molecular system under bias with or without a driving field; the electric field can result from a tip or, as here, be an external field. An important future direction is the study of nonlinear effects in weakly coupled systems.

We have identified a specific spectral region where each of the two components exhibits optical activity. In this region the weakly coupled system can interact via dipole-dipole coupling, and we indeed found sensitivity of the absorption lines to distance, even at large distances R. Once the distance between them is sufficiently reduced to about 0.7 nm, charge transfer excitations become increasingly important and the combination of increased sensitivity of the emission yield to R is observed. We have mentioned an additional handle on the system, namely, a bias potential, which is useful to fine tune the dipole-coupled resonances.

APPENDIX: THE $\gamma=1$ FUNCTIONAL

1. Time-independent DFT

We will not repeat here the derivation of the functional (see Ref. 53) and merely state the theorem that the exact ground-state energy can be written as a sum of density functionals:

$$E_{v,\mathcal{N}}[n] = T_s[n] + E_{\text{ext}}[n] + E_H[n] + E_X^\gamma[n] + E_{\text{XC}}^\gamma[n].$$

(A1)

The usual DFT terms such as $T_s[n]$, $E_{\text{ext}}[n]$, and $E_H[n]$ are, respectively, the noninteracting kinetic energy functional of Kohn and Sham and the energy associated with the electron-nuclear potential and the Hartree energy,

$$E_H[n] + \frac{1}{2}\int \frac{n(\mathbf{r})n(\mathbf{r}')}{|\mathbf{r}-\mathbf{r}'|}d^3rd^3r'.$$

(A2)

Also, an explicit Kohn-Sham exchange energy appears:

$$E_X^\gamma[n] = -\frac{1}{2}\int |P[n](\mathbf{r},\mathbf{r}')|^2 u_\gamma(|\mathbf{r}-\mathbf{r}'|)d^3rd^3r',$$

(A3)

with $P[n](\mathbf{r},\mathbf{r}')$ being the density matrix of noninteracting electrons having density n and

$$u_\gamma(r) = \frac{1-e^{-\gamma r}}{r}$$

(A4)

is a descreened electron-electron interaction potential. We proved that the descreening parameter γ is a density functional (i.e., it is a single-valued parameter depending on the density, $\gamma=\gamma[n]$). The last term is the new XC energy:

$$E_{XC}^{\gamma}[n] = \langle \Psi_{gs} | \hat{Y}_{\gamma} | \Psi_{gs} \rangle - \frac{1}{2} \int n(\mathbf{r}) n(\mathbf{r}')$$
$$\times y_{\gamma}(|\mathbf{r} - \mathbf{r}'|) d^3 r d^3 r', \qquad (A5)$$

where Ψ_{gs} is the exact ground-state wave function and $\hat{Y}_{\gamma} = 1/2 \Sigma_{i \ne j} y_{\gamma}(\hat{r}_{ij})$ with

$$y_{\gamma}(r) = e^{-\gamma r}/r. \qquad (A6)$$

The first approximation is to assume $\gamma[n]$ to be independent of the density and take a value of $\gamma = 1 a_0^{-1}$. The functional (A5) is then treated as a local density approximation, based on a Monte Carlo evaluation of the first term on the right of (A5) for a homogeneous electron gas. The result of this procedure gives

$$E_{XC}^{\gamma}[n] \approx \int \varepsilon_{XC}^{\gamma}(n(\mathbf{r})) n(\mathbf{r}) d^3 r, \qquad (A7)$$

with

$$\varepsilon_{XC}^{\gamma}(n) = \varepsilon_X^{\gamma}(n) + \varepsilon_C^{\gamma}(n), \qquad (A8)$$

and

$$\varepsilon_{XC}^{\gamma}(n) = -\frac{3k_F}{4\pi} H\left(\frac{\gamma}{k_F}\right), \qquad (A9)$$

where $k_F = (3\pi^2 n)^{1/3}$ is the Fermi momentum associated with density n and

$$H(q) = 1 - \frac{q^2}{6} - \frac{4q}{3} \tan^{-1}\left(\frac{2}{q}\right) + \frac{q^2}{24}(12 + q^2)\ln\left(\frac{4}{q^2} + 1\right) \qquad (A10)$$

is the exchange energy per particle of a homogeneous gas of particles of density n interacting via the force derived from Eq. (A4). Finally

$$\varepsilon_C^{\gamma}(n) = \eta_{\gamma}(\gamma r_s) \varepsilon_G(n), \qquad (A11)$$

where $\varepsilon_C(n)$ is the LSDA correlation energy and

$$\eta_{\gamma}(x) = \frac{C}{A_{\gamma}^0 + A_{\gamma}^1 x + x^2} + \frac{B}{A_{\gamma}^2 x^3 + A_{\gamma}^3 x^{3/2} + (A_{\gamma}^4 - \ln x)x}. \qquad (A12)$$

This form and selection of $C = 1.6976$, $B = 12.8$ ensure correct asymptotic $r_s \to \infty$ and $r_s \to 0$ limits. The low density behavior of η is determined from an analog of Wigner's theory for low density gas of particles interacting by a screened Coulomb potential[70] and the high density limit is based on correlation energy estimates given in Ref. 71. The parameters A_{γ}^i, $i = 0, \ldots, 4$, are determined using Monte Carlo calculations, as described in Ref. 53. For $\gamma = 1 a_0^{-1}$ and $0.8 a_0^{-1}$ they are given in Table II.

2. Time-dependent DFT

The application of the functional as a TD method can be done using the optimized effective potential method. This, however, is numerically costly and we make an approxima-

TABLE II. The parameters A_i for the γ functional.

i	$\gamma = 1 a_0^{-1}$	$\gamma = 0.8 a_0^{-1}$
0	5.377 083 59	4.327 613 43
1	−2.224 929 99	−1.796 749 68
2	0.140 242 88	0.180 797 73
3	7.090 280 96	2.531 119 42
4	15.675 084 16	23.052 568 19

tion by which the equations of motion are obtained by finding the stationary value of the following "noninteracting" action:

$$S[n] = \int_0^{t_l} \left\{ i \sum_{j=1}^{N_e} \langle \psi_j | \dot{\psi}_j \rangle - E_{v,N}[n(t)] \right\} dt, \qquad (A13)$$

producing Kohn-Sham equations for the N_e orbitals $\psi_j(\mathbf{r}, t)$ of the form

$$i\dot{\psi}_j(\mathbf{r}, t) = H_{KS}[n(t)](t)\psi_j(\mathbf{r}, t), \qquad (A14)$$

where $H_{KS}[n]$ is the Kohn-Sham Hamiltonian:

$$H_{KS} = T_s + v_{ext}(\mathbf{r}, t) + v_H(\mathbf{r}, t) + \hat{K}_X^{\gamma} + v_{XC}^{\gamma}(n(\mathbf{r}, t)), \qquad (A15)$$

while $v_{\parallel}(\mathbf{r}, t) = \int n(\mathbf{r}', t)/|\mathbf{r} - \mathbf{r}'| d^3 r'$ is the Hartree potential and

$$\hat{K}_X^{\gamma}\psi(\mathbf{r}, t) = -\int P(\mathbf{r}, \mathbf{r}', t)\psi(\mathbf{r}')u_{\gamma}(|\mathbf{r} - \mathbf{r}'|)d^3 r' \qquad (A16)$$

is the relevant exchange operator. Finally, $v_{XC}(n) = \varepsilon_{XC}^{\gamma}(n) + \varepsilon_{XC}^{\gamma\prime}(n)n$.

[1] E. Betzig and J. K. Trautman, Science **257**, 189 (1992).
[2] D. W. Pohl, W. Denk, and M. Lanz, Appl. Phys. Lett. **44**, 651 (1984).
[3] R. C. Dunn, Chem. Rev. (Washington, D.C.) **99**, 2891 (1999).
[4] C. Hubert, A. Rumyantseva, G. Lerondel et al., Nano Lett. **5**, 615 (2005).
[5] D. Courjon and C. Bainier, Rep. Prog. Phys. **57**, 989 (1994).
[6] C. Girard, Rep. Prog. Phys. **68**, 1883 (2005).
[7] P. F. Barbara, D. M. Adams, and D. B. O'Connor, Annu. Rev. Mater. Sci. **29**, 433 (1999).
[8] A. Lewis, H. Taha, A. Strinkovski, A. Manevitch, A. Khatchatouriants, R. Dekhter, and E. Ammann, Nat. Biotechnol. **21**, 1377 (2003).
[9] A. Cricenti, R. Generosi, M. Luce et al., Biophys. J. **85**, 2705 (2003).
[10] T. W. Ebbesen, H. J. Lezec, H. F. Ghaemi, T. Thio, and P. A. Wolff, Nature (London) **391**, 667 (1998).
[11] S. A. Maier, M. L. Brongersma, P. G. Kik, S. Meltzer, A. A. G. Requicha, B. E. Koel, and H. A. Atwater, Adv. Mater. (Weinheim, Ger.) **15**, 562 (2003).
[12] A. Nitzan and L. E. Brus, J. Chem. Phys. **75**, 2205 (1981).
[13] B. T. Draine and P. J. Flatau, J. Opt. Soc. Am. A **11**, 1491 (1994).
[14] A. Taflove and S. C. Hagness, Computational Electrodynamics: The Finite-Difference Time-Domain Method, 2nd ed. (Artech House, Boston, 2000).
[15] J. Fiurasek, B. Chernobrod, Y. Prior, and I. S. Averbukh, Phys. Rev. B **63**, 045420 (2001).
[16] K. G. Stephen and K. Teobald, Phys. Rev. B **68**, 045415 (2003).
[17] T. W. Lee and S. K. Gray, Appl. Phys. Lett. **86**, 141105 (2005).
[18] S. H. Chang, S. K. Gray, and G. C. Schatz, Opt. Express **13**, 3150 (2005).
[19] S. Bruzzone, M. Malvaldi, G. P. Arrighini, and C. Guidotti, J. Phys. Chem. B **109**, 3807 (2005).
[20] S. A. Maier, P. G. Kik, and H. A. Atwater, Phys. Rev. B **67**, 205402 (2003).
[21] C. F. Bohren and D. R. Huffman, Absorption and Scattering of Light by Small Particles (Wiley, New York, 1983).

[22] S. Gresillon, H. Cory, J. C. Rivoal, and A. C. Boccara, J. Opt. A, Pure Appl. Opt. **1**, 178 (1999).

[23] J. C. Weeber, A. Dereux, C. Girard, G. C. des Francs, J. R. Krenn, and J. P. Goudonnet, Phys. Rev. E **62**, 7381 (2000).

[24] V. Sandoghdar, J. Michaelis, C. Hettich, C. Schmitt, J. Zitzmann, and S. Kühn, Single Mol. **2**, 277 (2001).

[25] M. Brun, A. Drezet, H. Mariette, N. Chevalier, J. C. Woehl, and S. Huant, Europhys. Lett. **64**, 634 (2003).

[26] N. Chevalier, M. J. Nasse, J. C. Woehl, P. Reiss, J. Bleuse, F. Chandezon, and S. Huant, Nanotechnology **16**, 613 (2005).

[27] W. L. Barnes, A. Dereux, and T. W. Ebbesen, Nature (London) **424**, 824 (2003).

[28] D. J. Sirbuly, M. Law, P. Pauzauskie, H. Q. Yan, A. V. Maslov, K. Knutsen, C. Z. Ning, R. J. Saykally, and P. D. Yang, Proc. Natl. Acad. Sci. U.S.A. **102**, 7800 (2005).

[29] M. Law, D. J. Sirbuly, J. C. Johnson, J. Goldberger, R. J. Saykally, and P. D. Yang, Science **305**, 1269 (2004).

[30] T. Maniv and H. Metiu, Phys. Rev. B **22**, 4731 (1980).

[31] K. Burke, J. Werschnik, and E. K. U. Gross, J. Chem. Phys. **123**, 062206 (2005).

[32] A. Zangwill and P. Soven, Phys. Rev. A **21**, 1561 (1980).

[33] E. K. U. Gross and W. Kohn, Phys. Rev. Lett. **55**, 2850 (1985).

[34] R. Baer and D. Neuhasuer, J. Chem. Phys. **121**, 9803 (2004).

[35] J. R. Chelikowsky, L. Kronik, and I. Vasiliev, J. Phys.: Condens. Matter **15**, R1517 (2003).

[36] K. Yabana and G. F. Bertsch, Phys. Rev. B **54**, 4484 (1996).

[37] R. Baer, Phys. Rev. A **62**, 063810 (2000).

[38] F. Calvayrac, P. G. Reinhard, E. Suraud, and C. A. Ullrich, Phys. Rep. **337**, 493 (2000).

[39] R. Baer and R. Gould, J. Chem. Phys. **114**, 3385 (2001).

[40] R. Baer, S. Weiss, and D. Neuhauser, Nano Lett. **4**, 85 (2004).

[41] R. Baer and N. Siam, J. Chem. Phys. **121**, 6341 (2004).

[42] S. Kallush, Y. Band, and R. Baer, Chem. Phys. Lett. **392**, 23 (2004).

[43] R. Baer, Y. Kurzweil, and L. S. Cederbaum, Isr. J. Chem. **45**, 161 (2005).

[44] P. G. Reinhard and E. Suraud, Laser Phys. **11**, 566 (2001).

[45] X. M. Tong and S. I. Chu, Phys. Rev. A **64**, 013417 (2001).

[46] C. A. Ullrich, U. J. Gossmann, and E. K. U. Gross, Ber. Bunsenges. Phys. Chem. **99**, 488 (1995).

[47] R. Baer, D. Neuhauser, P. Zdanska, and N. Moiseyev, Phys. Rev. A **68**, 043406 (2003).

[48] M. Lein and S. Kummel, Phys. Rev. Lett. **94**, 143003 (2005).

[49] S. Kummel, K. Andrae, and P. G. Reinhard, Appl. Phys. B: Lasers Opt. **73**, 293 (2001).

[50] F. Calvayrac, A. Domps, P. G. Reinhard, E. Suraud, and C. A. Ullrich, Eur. Phys. J. D **4**, 207 (1998).

[51] Y. Kurzweil and R. Baer, Phys. Rev. B **73**, 075413 (2006).

[52] R. Baer, T. Seideman, S. Ilani, and D. Neuhauser, J. Chem. Phys. **120**, 3387 (2004).

[53] R. Baer and D. Neuhauser, Phys. Rev. Lett. **94**, 043002 (2005).

[54] H. Iikura, T. Tsuneda, T. Yanai, and K. Hirao, J. Chem. Phys. **115**, 3540 (2001).

[55] M. Kamiya, H. Sekino, T. Tsuneda, and K. Hirao, J. Chem. Phys. **122**, 234111 (2005).

[56] T. Brixner, F. J. G. de Abajo, J. Schneider, and W. Pfeiffer, Phys. Rev. Lett. **95**, 093901 (2005).

[57] B. M. Reinhard, M. Siu, H. Agarwal, A. P. Alivisatos, and J. Liphardt, Nano Lett. **5**, 2246 (2005).

[58] C. Sonnichsen, B. M. Reinhard, J. Liphard, and A. P. Alivisatos, Nat. Biotechnol. **23**, 741 (2005).

[59] Y. Ebenstein, E. Yoskovitz, R. Costi, A. Aharoni, and U. Banin, J. Phys. Chem. A **110**, 8297 (2005).

[60] C. Hettich, C. Schmitt, J. Zitzmann, S. Kuhn, I. Gerhardt, and V. Sandoghdar, Science **298**, 385 (2002).

[61] G. J. Martyna and M. E. Tuckerman, J. Chem. Phys. **110**, 2810 (1999).

[62] W. H. Press, S. A. Teukolsky, W. T. Vetterling, and B. P. Flannery, *Numerical Recipes in C.* (Cambridge University Press, Cambridge 1992).

[63] W. Kohn and L. J. Sham, Phys. Rev. **140**, A1133 (1965).

[64] J. P. Perdew, R. G. Parr, M. Levy, and J. L. Balduz, Phys. Rev. Lett. **49**, 1691 (1982).

[65] M. Brack, Rev. Mod. Phys. **65**, 677 (1993).

[66] W. Ekardt, Phys. Rev. Lett. **52**, 1925 (1984).

[67] U. von Barth and C.-O. Almbladh, Phys. Rev. B **31**, 3231 (1985).

[68] A. Dreuw, J. L. Weisman, and M. Head-Gordon, J. Chem. Phys. **119**, 2943 (2003).

[69] R. Eisenschitz and F. London, Z. Phys. **60**, 491 (1930).

[70] E. Wigner, Phys. Rev. **46**, 1002 (1934).

[71] V. A. Rassolov, J. A. Pople, and M. A. Ratner, Phys. Rev. B **59**, 15625 (1999).